DOI: 10.24352/UB.OVGU-2017-082 TECHNISCHE MECHANIK, 37, 1, (2017), 62 – 68
submitted: May 19, 2017

Experimental Study on the Velocity Dependent Drag Coefficient and Friction in an Automatic Ball Balancer

L. Spannan, C. Daniel, E. Woschke

The paper presents the evaluation of experiments on the drag and friction forces in an automatic ball balancer, which raceway is embodied by the outer ring of a ball-bearing. Due to the throughout contact between the balls and the raceway while operating the ball balancer, effort has been made to characterise the flow conditions of the surrounding fluid by determining the drag coefficient C_D as a function of the Reynolds number Re*. By the use of fluids with different viscosities and the postulation of continuity in the run of C_D*(Re)*, coefficients for different friction models, e.g. Coulomb friction and rolling friction deduced from Hertzian surface pressure equation can be derived.*

1 Introduction

With automatic ball balancers the vibrations due to process dependent variable unbalances, e.g. in centrifuges, can be reduced. Free movable balls are located in a raceway, which geometric center $\mathcal{O}_G$ is coinciding at rest with the center of rotation $\mathcal{O}_R$. While rotating at super-critical speeds, the residuals of normal forces F_N and centrifugal forces F_{cf} on the balls move them towards their stable stationary position opposite to the unbalance location, which results in the reduction of the overall unbalance in the rotor, fig. 1.

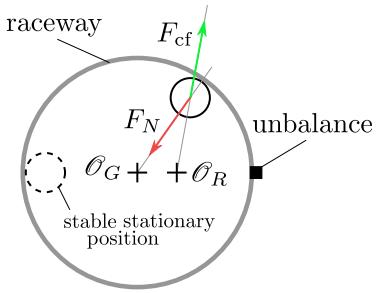

Figure 1: Schematic representation of a ball balancer at super-critical speed in the rotating reference frame.

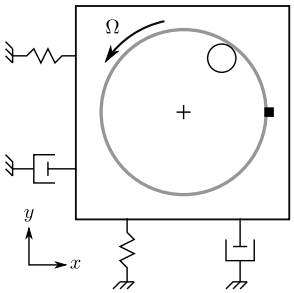

Figure 2: Rotor with a ball balancer suspended by linear springs and dampers in the inertial reference frame.

The efficiency of automatic ball balancers depends on several parameters, which are chosen in the design process. The maximum unbalance, which can be compensated, is determined by the mass m_b of the balls, the radius R_b of the balls' centroidal track and the accuracy with which the ideal stationary position can be reached. The latter is influenced by friction between the balls and the raceway as well as shape and positional deviations of the raceway compared to an ideal circle with its center on the shaft axis.

Another aspect of the design process is the choice of the fluid in which the balls are environed. The kinematic viscosity ν_{fl} and the density ϱ_{fl} of the fluid, the friction as well as the flow conditions, e.g. drag and displacement forces, determine the speed with which the stationary position is attained. Because the balls are forced in the direction of unbalance at sub-critical speeds and therefore worsening the unbalance situation, a compromise has to be met with respect to the run-up process. Depending on the acceleration of the run-up, the aforementioned parameters should be chosen in a way, that the balls lag behind the rotor speed at sub-critical speeds and catch up to the rotor speed reaching the stationary position quickly at super-critical speeds (Ryzhik et al. (2003)).

In order to simulate the run-up and identify suitable fluid properties, models for drag and friction as well as proper

coefficients are necessary. The presented study identifies the velocity-drag correlation for the presented rotor and derives friction coefficients from the experimental data.

2 State of Research

Stationary solutions of the dynamics of automatic ball balancers with a focus on stability (e.g. Green et al. (2006), Ishida et al. (2012), Kim and Na (2013)) often use the linear correlation to model the viscous coupling between the rotational speeds $\dot{\varphi}_R$ and $\dot{\varphi}_b$ of the rotor and the ball and the drag moment

$$M_D = \beta \cdot (\dot{\varphi}_R - \dot{\varphi}_b) \, .$$

The difficulty lies in the quantitative identification of the parameter β. A physically motivated approach based on the drag force

$$F_D = \frac{1}{2} \varrho_{\mathrm{fl}} \cdot \bar{A} \cdot C_D \cdot v_{\mathrm{rel}}^2 \cdot \mathrm{sign}(v_{\mathrm{rel}}) \tag{1}$$

and therefore

$$M_D = F_D \cdot R_b = \frac{1}{2} \varrho_{\mathrm{fl}} \cdot \bar{A} \cdot C_D \cdot v_{\mathrm{rel}}^2 \cdot R_b \cdot \mathrm{sign}(v_{\mathrm{rel}}) \tag{2}$$

was used by Huang et al. (2002). $\bar{A}$, C_D, v_{rel} describe the balls cross-sectional area, the drag coefficient and the flow velocity, respectively. The latter can be approximated by

$$v_{\mathrm{rel}} \approx \Omega \cdot R_b \tag{3}$$

for $d/R_b << 1$.

As can be seen from varying flow velocities detected in run-up experiments (Spannan et al. (2017)), the assumption that the drag coefficient C_D is constant should be discarded in favor of a flow velocity dependent formulation depending on the Reynolds number Re. Due to the continuous contact between the ball and the raceway, the empirically determined correlation of Jan and Chen (1997),

$$C_D(\mathrm{Re}) = \begin{cases} 322/\,\mathrm{Re} & \text{if } \mathrm{Re} \leq 10 \\ 10^{3.02 - 1.89\log(\mathrm{Re}) + 0.411(\log(\mathrm{Re}))^2 - 0.033(\log(\mathrm{Re}))^3} & \text{if } 10 < \mathrm{Re} \leq 20000 \\ 0.74 & \text{if } \mathrm{Re} > 20000 \, , \end{cases} \tag{4}$$

was checked as a suitable approximation. In the tests an outer ring of a ball-bearing 6926 is used as the raceway and the bearing balls are used as the counterbalancing masses leading to a concave contact surface and low friction. Furthermore, the dimensions of the cross-section of the annulus, which contains the fluid and the balls, are in the magnitude of the ball diameter, which can influence the drag due to the close boundaries. The following experimental results show the correlation $C_D(\mathrm{Re})$ for the specific discoidal rotor in use, whose half-section is depicted in fig. 3 and dimensions are given in tab. 1.

One method to model the friction between the ball and the raceway is the Coulomb friction force $F_R = \mu F_N$ proportional to the normal force and acting in the contact point opposing the direction of movement. However, as stated by Ishida et al. (2012), the Coulomb friction model is not capable to explain all characteristics in a ball balancer. A rolling friction model based on the Hertzian surface pressure was derived by Chao et al. (2005),

$$M_f(\alpha_0) = \frac{3}{16} F_N^{\frac{4}{3}} \cdot \left(\frac{3}{d^2} \right)^{\frac{1}{3}} \cdot \alpha_0 \cdot \left(\frac{1 - \nu^2}{E} \right)^{\frac{1}{3}} \, , \tag{5}$$

modelling the balls as rigid bodies and the raceway as a flexible flat yielding surface with Young's modulus E and Poisson's ratio ν. The factor α_0 serves as a fitting parameter to account for example for the surface roughness.

Table 1: Properties of the ball balancer under consideration.

description	symbol	dimension
ball diameter	d	12.3 mm
radius of the ball's centroidal track	R_b	76.95 mm
height of the annulus cross-section	H	20 mm
width of the annulus cross-section	W	13.8 mm

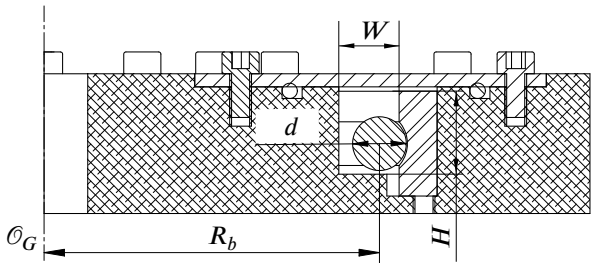

Figure 3: Half-section of the discoidal rotor containing the outer ring of a ball-bearing.

3 Conducted Experiments

In order to derive the velocity-drag correlation for the presented ball balancer, the rotor is mounted on a horizontal shaft, which is driven by an electric motor, fig. 4. An incremental encoder is used to measure the rotor speed Ω. The rotor speed is changed quasi statically, leaving the ball in an equilibrium between the gravitational force, the drag and the friction at a specific angle γ. The rotor speed was varied in such a way that the equilibrium angle γ covers the sector from 0° to 90°.

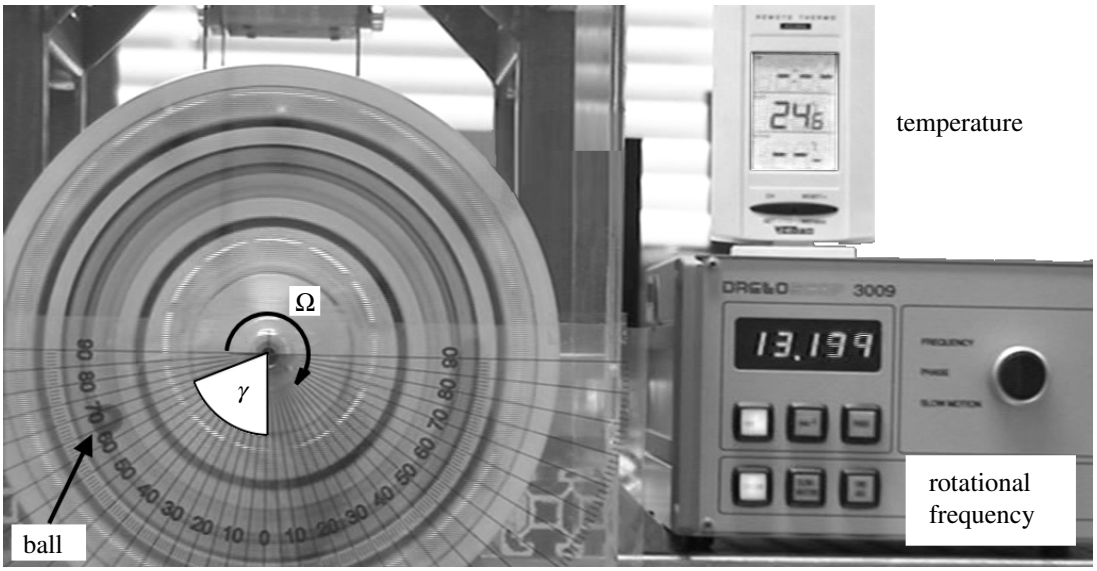

Figure 4: Setup of the test rig.

Depending on the chosen friction model, fig. 5 and fig. 6, either balance of force and moment at the contact point f can be evaluated to gain the correlation between the drag coefficient C_D and the Reynolds number

$$\mathrm{Re} = \frac{v_{\mathrm{rel}} \cdot d}{\nu_{\mathrm{fl}}} \approx \frac{\Omega \cdot R_b \cdot d}{\nu_{\mathrm{fl}}} \,. \tag{6}$$

The buoyancy is considered by a reduced mass of the steel balls

$$m_{\mathrm{eff}} = \frac{\pi}{6} d^3 \cdot (\varrho_b - \varrho_{\mathrm{fl}}) \quad .$$

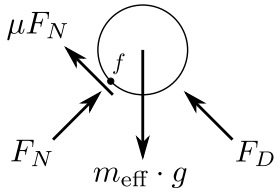

Figure 5: Forces on the ball with Coulomb friction.

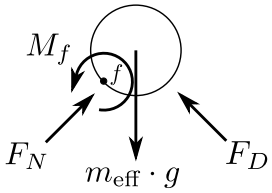

Figure 6: Forces on the ball with Hertz rolling friction.

Evaluation of the balance equations leads with eq. (1) and eq. (2) respectively to

$$C_D = \frac{2 \cdot m_{\text{eff}} \cdot g \cdot \sin(\gamma)}{\varrho_{\text{fl}} \cdot \bar{A} \cdot \Omega^2 \cdot R_b^2} \qquad \text{neglecting friction,} \tag{7}$$

$$C_D = \frac{2 \cdot m_{\text{eff}} \cdot g(\sin(\gamma) - \mu \cos(\gamma))}{\varrho_{\text{fl}} \cdot \bar{A} \cdot \Omega^2 \cdot R_b^2} \qquad \text{with Coulomb friction and} \tag{8}$$

$$C_D = \frac{2(m_{\text{eff}} \cdot g \cdot \frac{d}{2} \cdot \sin(\gamma) - M_f)}{\frac{d}{2} \cdot \varrho_{\text{fl}} \cdot \bar{A} \cdot \Omega^2 \cdot R_b^2} \qquad \text{with rolling friction.} \tag{9}$$

Different fluids were used in order to cover a broader range of Reynolds numbers, tab. 2, according to eq. (6). Two motor oils, whose kinematic viscosities at room temperature were derived from their viscosity indices, and two silicone oils with nominal kinematic viscosities $\nu_{\text{fl}} = 0.65\,\text{mm}^2\,\text{s}^{-1}$ and $50\,\text{mm}^2\,\text{s}^{-1}$, respectively. The set was supplemented by blendings of the silicone oils aiming at kinematic viscosities of $\nu_{\text{fl}} = 2$, 5, 10, and $20\,\text{mm}^2\,\text{s}^{-1}$, starting with the least viscous oil ($\nu_{\text{fl}} = 0.65\,\text{mm}^2\,\text{s}^{-1}$) and adding the high viscous oil subsequently. The necessary blending fractions were derived from the Arrhenius equation for the viscosity of ideal binary mixtures (Zhmud (2014))

$$\ln(\nu_{12}\varrho_{12}) = x_1 \ln(\nu_1\varrho_1) + (1 - x_1)\ln(\nu_2\varrho_2) \quad . \tag{10}$$

With $\varrho_{12} \approx \frac{\varrho_1+\varrho_2}{2}$ the necessary blending fraction in order to obtain the desired kinematic viscosities yields

$$x_1 = \frac{\ln(\nu_{12}\frac{\varrho_1+\varrho_2}{2}) - \ln(\nu_2\varrho_2)}{\ln(\nu_1\varrho_1) - \ln(\nu_2\varrho_2)} \quad . \tag{11}$$

The final blend aiming at $\nu_{\text{fl}} = 20\,\text{mm}^2\,\text{s}^{-1}$ was checked with a viscometer resulting to $\nu_{\text{fl}} = 23\,\text{mm}^2\,\text{s}^{-1}$, which supports the approximation eq. (11) and the conducted blending procedure. On the basis of these fluid properties different sectors of Reynolds numbers are covered, which are overlapping each other partially.

Table 2: Properties of the fluids used in the experiments.

fluid	density ϱ_{fl} [kg m^{-3}]	kinematic viscosity ν_{fl} [mm^2 s^{-1}]	
Ravenol® 80W	886	214	nominal
ADDINOL® SD-Oil B 5W	836	31	nominal
silicone oil 0.65	760	0.65	nominal
silicone oil 50	950	50	nominal
silicone oil 2	800	2	as of eq. (10)
silicone oil 5	844	5	as of eq. (10)
silicone oil 10	876	10	as of eq. (10)
silicone oil 20	939	23	measured

4 Results

The correlation between the drag coefficient C_D and the Reynolds number Re are derived from the measured rotational frequency and equilibrium angle γ and equations (6) and (7-9). The results are depicted in figures 7 to 9. The dashed line represents the speed dependent drag on a sphere in a free flow environment, published by Morrison

(2013). The solid line depicts the correlation for a sphere in contact with a flat surface, eq. (4). By neglecting any form of friction the experimental data shown in fig. 7 results from eq. (7). The data shows an adequate agreement with the flat surface contact condition but the overlap of the different data sets is not satisfactory.

The results at high velocities are not coinciding with the low velocity data of the subsequent data set due to the neglect of friction. Because of higher normal forces F_N at lower speeds (small angles γ) the influence of friction is most significant at small Reynolds numbers for each data set. The influence of friction can be seen clearly from fig. 8 where equations (8) and (9) are evaluated with overestimated friction coefficients μ for the Coulomb friction model and $\alpha_0 \left(\frac{1-\nu^2}{E}\right)^{\frac{1}{3}}$ for the Hertz rolling friction model.

By fitting the friction coefficients a satisfying overlap of the experimental data sets can be accomplished, fig. 9. Remaining deviations are still present for the data with large angles γ, which show decreasing trends of drag. It is assumed that, due to small radial forces at angles near 90°, the lift forces cause the ball to detach from the raceway leading to a gap, which reduces the drag. This assumption coincides with the observations made during the experiments.

5 Conclusions

The main focus of this work was to obtain a $C_D - \mathrm{Re}$ relation for the flow conditions in automatic ball balancers. Concluding from the experimental data, the drag resulting from the flow around a ball in the automatic ball balancer can be described approximately by equation (4). Residual deviations to higher drag forces due to the concave contact and the annulus geometry may be considered by correction factors, if necessary. This will be the case for smaller balancer dimensions in relation to the ball diameter, presumably.

Furthermore, friction has to be considered in order to interpret the data and obtain continuous experimental results in the $C_D - \mathrm{Re}$ diagram. Approximations for the friction coefficients are determined in order to meet this criterion. In comparison to the friction coefficients provided by Chao et al. (2005), the presented coefficient exceeds by a factor of 1000, tab. 3. The discrepancy is assumed to result from the relatively small normal forces acting on the ball. In relation to gravitational forces acting on the ball, the presented setup can only provide normal forces with a factor of $F_N/(m_b \cdot g) \leq 1$, whereas possible applications deal with centrifugal forces between $100\,g$ and $100\,000\,g$, tab. 3. Nevertheless, the presented data can be used to validate simulation models of ball balancers at low speeds with a focus on the drag characteristics.

Table 3: Evaluation of the derived friction coefficient with respect to the normal forces.

	determination		application			
	present study	Chao et al. (2005)	Spannan et al. (2017)	CD-ROM drive	micro centrifuges	superspeed centrifuges
$F_N/(m_b \cdot g)$	0 … 1	1166	38	950	20 000	100 000
$\alpha_0 \left(\frac{1-\nu^2}{E}\right)^{\frac{1}{3}}$	1.5×10^{-4}	0.8×10^{-7}				

6 Future prospects

Providing the verified drag relation between the fluid and the ball in an automatic ball balancer, transient simulations can be modelled more precisely. Based on the broad range of viscosities and densities of the fluid medium used, these simulations can enhance the design process of efficient automatic ball balancers.

Based on the presented modelling approach for the viscous coupling between the rotor and the balancing masses, transient simulations will be conducted and compared to ball movements extracted from video recordings of run-up experiments in subsequent studies.

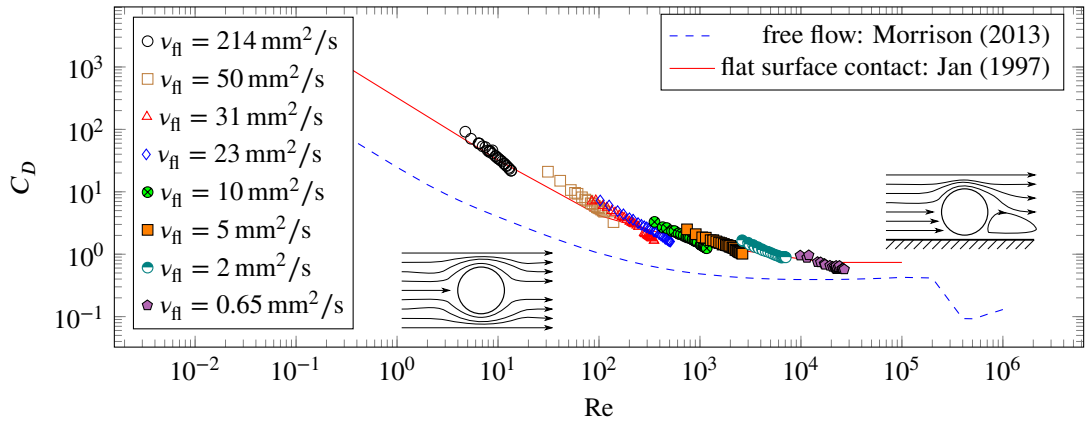

Figure 7: Drag coefficient of flow around a ball for different kinematic viscosities ν_{fl} in an automatic ball balancer with a bearing raceway. Friction is neglected according to eq. (7).

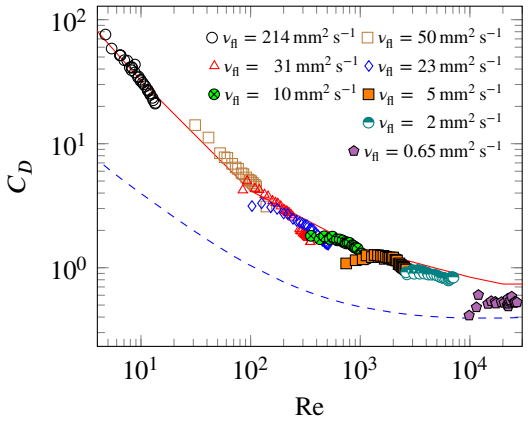

(a) Coulomb friction with $\mu = 0.10$

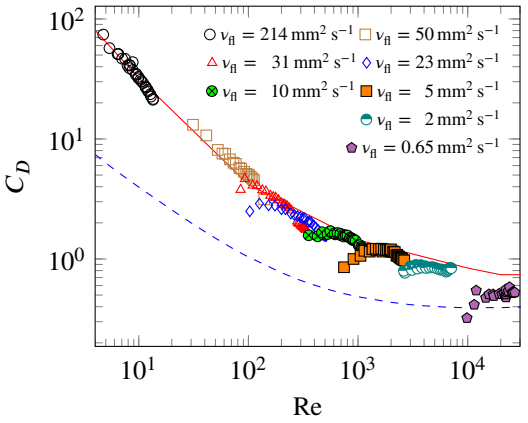

(b) Hertz rolling friction with $\alpha_0 \left(\frac{1-\nu^2}{E}\right)^{\frac{1}{3}} = 3.5 \times 10^{-4}$

Figure 8: Influence of overestimated friction coefficients on the run of the drag coefficient.

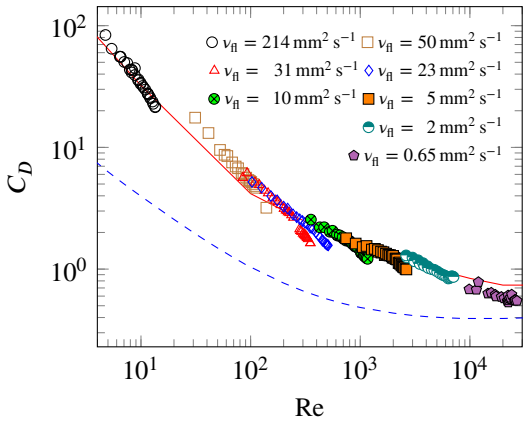

(a) Coulomb friction with $\mu = 0.05$

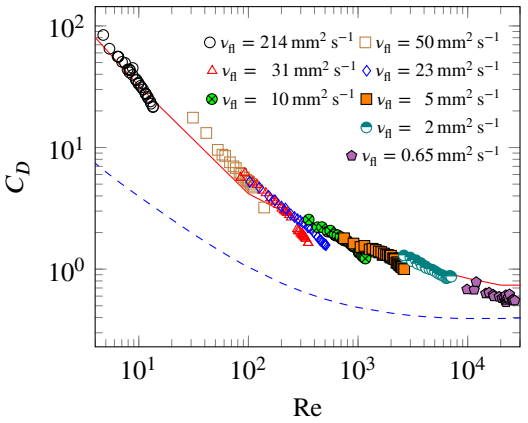

(b) Hertz rolling friction with $\alpha_0 \left(\frac{1-\nu^2}{E}\right)^{\frac{1}{3}} = 1.5 \times 10^{-4}$

Figure 9: Run of the drag coefficient with fitted friction coefficients.

Acknowledgments

Funded by the German Federal Ministry of Economics and Energy. The support of Mr. Samuel Voß, University of Magdeburg (ISUT), in conducting the viscosity measurements is greatly appreciated.

References

Chao, P. C.-P.; Sung, C.-K.; Leu, H.-C.: Effects of rolling friction of the balancing balls on the automatic ball balancer for optical disk drives. *Journal of Tribology*, 127, 4, (2005), 845.

Green, K.; Champneys, A.; Friswell, M.: Analysis of the transient response of an automatic dynamic balancer for eccentric rotors. *International Journal of Mechanical Sciences*, 48, 3, (2006), 274–293.

Huang, W.; Chao, C.; Kang, J.; Sung, C.: The application of ball-type balancers for radial vibration reduction of high-speed optic disk drives. *Journal of Sound and Vibration*, 250, (2002), 415–430.

Ishida, Y.; Matsuura, T.; Zhang, X. L.: Efficiency improvement of an automatic ball balancer. *J. Vib. Acoust.*, 134, 2, (2012), 021012.

Jan, C.-D.; Chen, J.-C.: Movements of a sphere rolling down an inclined plane. *Journal of Hydraulic Research*, 35, 5, (1997), 689–706.

Kim, T.; Na, S.: New automatic ball balancer design to reduce transient-response in rotor system. *Mechanical Systems and Signal Processing*, 37, 1-2, (2013), 265–275.

Morrison, F. A.: *An introduction to fluid mechanics*. Cambridge University Press (2013).

Ryzhik, B.; Sperling, L.; Duckstein, H.: The influence of damping on the efficiency of autobalancing devices for rigid rotors. In: *Proceedings of The Second International Symposium on Stability Control of Rotating Machinery ISCORMA-2003*, pages 104–113, Gdańsk, Poland (2003).

Spannan, L.; Daniel, C.; Woschke, E.: Run-up simulation of automatic balanced rotors considering velocity-dependent drag coefficients. In: *SIRM 2017 - 12th International Conference on Vibrations in Rotating Machines*, Graz, Austria (Feb. 2017).

Zhmud, B.: Viscosity blending equations. *Lube-Tech*, 121, 93, (2014), 22–27.

Address: L. Spannan, C. Daniel, E. Woschke
IFME, Otto-von-Guericke-Universität Magdeburg, Universitätsplatz 2, 39106 Magdeburg, Deutschland
email: {lars.spannan,christian.daniel,elmar.woschke}@ovgu.de